A Review of Cermet-based Spectrally Selective Solar Absorbers

Feng Cao,[a] Kenneth McEnaney,[b] Gang Chen,[*b] and Zhifeng Ren*[a]

[a] Department of Physics and TcSUH, University of Houston, Houston, Texas 77204, USA

[b] Department of Mechanical Engineering, Massachusetts Institute of Technology, Cambridge, Massachusetts 02139, USA

To whom correspondence should be addressed, gchen2@mit.edu, zren@uh.edu

Abstract

Spectrally-selective solar absorbers harvest solar energy in the form of heat. Solar absorbers using cermet-based coatings demonstrate a high absorptance of the solar spectrum and a low emittance in the infrared (IR) regime. Extensive work has been done to optimize cermet-based solar absorbers to achieve high performance by exploring different cermet (ceramic-metal composite) materials and film configurations through different preparation techniques such as electrodeposition, sputtering, pulsed laser deposition, and solution-based methods. In this article, we review the progress of cermet-based spectrally-selective absorbers with high solar absorptance and low thermal emittance, such as Cr_2O_3, Al_2O_3, AlN, SiO_2, and ZrO_2 based cermets as absorption layers. We also present an outlook for cermet-based spectrally-selective absorbers with high thermal stability and high conversion efficiency from sunlight to heat.

Nomenclature

α_s	Solar absorptance
ε'_λ	Spectral directional emittance
ε_t	Thermal emittance
η_{abs}	Absorber efficiency
σ_{sb}	Stefan-Boltzmann constant
H_{abs}	Incident solar flux
h_{conv}	Convective heat transfer coefficient
$I_{b\lambda}$	Spectral blackbody intensity
q_c	Waste heat

q_{conv}	Convective loss
q_h	Heat flux
q_{rad}	Radiative loss
S	Incident solar intensity
AM	Air mass
ARC	Anti-reflection coating
CSP	Concentrated solar power
CVD	Chemical vapor deposition
DC	Direct current
FTIR	Fourier transform infrared spectroscopy
HMVF	High metal volume fraction
IR	Infrared
LHL	L: low metal fraction in cermet; H: high metal fraction in cermet
LMVF	Low metal volume fraction
MNS	Molybdenum-coated nickel-plated stainless steel
PV	Photovoltaics
PVD	Physical vapor deposition
RF	Radio frequency
SS	Stainless steel
STEG	Solar thermoelectric generators
STPV	Solar thermophotovoltaics
TISS	Thickness-insensitive spectrally selective
TSSS	Thickness-sensitive spectrally selective
UV	Ultraviolet
XRD	X-ray diffraction

1. Introduction

The drive to replace fossil fuels with renewable energy sources such as solar and wind was accelerated by the energy crisis of the 1970s[1]. Solar energy is abundant, striking the earth at a rate of 90,000 TW, which is 5,000 times our current global power consumption[2]. Generally there are two routes for harvesting solar energy: photovoltaics (PV)[3] and thermal processes. Photovoltaic conversion is the most widespread solar-to-electricity technology, with over 100 GW installed to date[4]. Thermal processes encompass a wide variety of technologies, all of which begin by converting the incident sunlight to heat. This heat can be converted to electricity, as is currently done in concentrated solar power (CSP) plants via a Rankine or combined cycle[5], solar

thermoelectric generators (STEG)[6], and solar thermophotovoltaics (STPV)[7, 8]. Currently there are 3 GW of installed and under-construction CSP plants in the world, but STEGs and STPV have yet to be commercialized. Solar thermal energy, or the waste heat from the aforementioned solar-to-electricity processes, can also be used for heating or cooling. Nearly 300 GW of solar thermal heat or hot water systems have been installed worldwide[7].

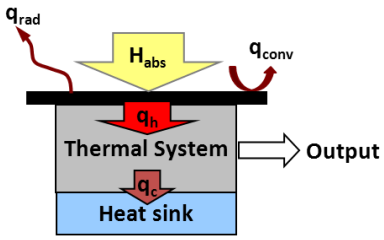

Fig. 1. A typical solar thermal energy conversion system. Sunlight incident on the absorber (H_{abs}) is converted to a heat flux (q_h) and delivered to the thermal system, where the desired output (work, electricity, heat, cooling, etc.) is produced. Waste heat (q_c) may be generated in the process and rejected to a heat sink. Radiative (q_{rad}) and convective (q_{conv}) losses at the surface reduce the potential output of the system.

A schematic of a typical solar thermal to electrical energy conversion system is shown in Fig. 1. In such solar thermal technologies, the sunlight is absorbed as heat at the absorber. This absorber must strongly absorb the sunlight, while ideally losing little heat to the environment via convection and radiation. An absorber which has strong solar absorptance and low infrared (IR) emittance is called a spectrally-selective absorber[9, 10]. In this review, we focus on spectrally-selective absorbers based on cermets, which are mixtures of ceramics and metals. When integrated with an anti-reflection coating (ARC) and an IR-reflective base layer (either an intrinsically IR-reflecting substrate or an IR-reflective coating on a substrate), cermet-based coatings (Fig. 2) can be very effective spectrally-selective absorbers.

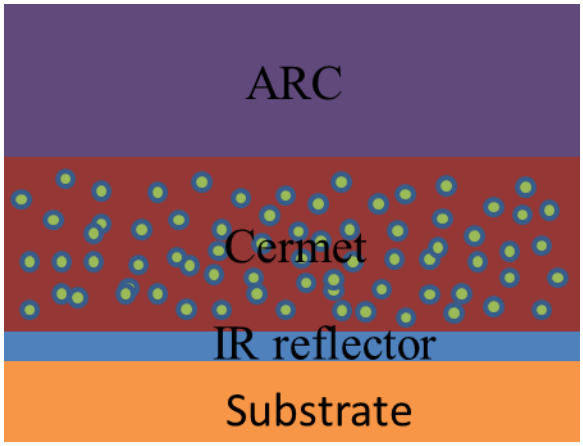

Fig. 2. Schematic representation of a cermet-based spectrally-selective absorber. The anti-reflection coating (ARC) reduces solar reflection off the surface; the cermet provides selective absorption; and the IR reflector (typically Cu, Al, Mo, or other metal with low intrinsic emissivity) reduces radiation losses. The substrate is usually metal (to conduct heat well) or glass (for lower cost). The cermet comprises a dielectric host (dark red) with metal particle inclusions (circles).

In this review, we begin by summarizing the requirements for solar selectivity, as well as the metrics for evaluating absorbers. We then review the preparation techniques, materials, and performance of cermet-based spectrally-selective absorbers. Finally we present the future outlook for cermet-based absorbers.

2. Selective Absorber Theory

Absorbers must efficiently convert a solar flux into heat, and deliver that heat to the thermal system (Fig. 1). The efficiency of the conversion from solar irradiance at the absorber, H_{abs}, to a heat flux delivered to the thermal system, q_h, is defined as the absorber efficiency, η_{abs}:

$$\eta_{abs} = \frac{q_h}{H_{abs}} = \alpha_s - \varepsilon_t \frac{\sigma_{sb}\left(T_h^4 - T_{amb}^4\right)}{H_{abs}} - \frac{h_{conv}(T_h - T_{amb})}{H_{abs}} \quad (1)$$

where σ_{sb} is the Stefan-Boltzmann constant, T_h is the absorber temperature, T_{amb} is the temperature of the environment, and h_{conv} is the convective heat transfer coefficient. The solar absorptance, α_s, is defined as:

$$\alpha_s = \frac{\int_0^{\infty}\int_0^{2\pi}\int_0^{\pi/2} \varepsilon'_{\lambda}(\lambda,\phi,\theta) S(\lambda,\phi,\theta)\cos\theta\sin\theta d\lambda\, d\phi\, d\theta}{\int_0^{\infty}\int_0^{2\pi}\int_0^{\pi/2} S(\lambda,\phi,\theta)\cos\theta\sin\theta d\lambda\, d\phi\, d\theta} \quad (2)$$

where λ is the wavelength of radiation, ϕ is the azimuthal angle, θ is the polar angle, ε'_{λ} is the spectral directional emittance at the operational temperature, and S is the incident solar intensity at the absorber. The numerator of this equation is the total absorbed solar energy; the denominator is the incident solar flux H_{abs}.

The thermal emittance, ε_t, is defined as:

$$\varepsilon_t = \frac{\int_0^{\infty}\int_0^{2\pi}\int_0^{\pi/2} \varepsilon'_{\lambda}(\lambda,\phi,\theta) I_{b\lambda}(\lambda,\phi,\theta)\cos\theta\sin\theta d\lambda\, d\phi\, d\theta}{\int_0^{\infty}\int_0^{2\pi}\int_0^{\pi/2} I_{b\lambda}(\lambda,\phi,\theta)\cos\theta\sin\theta d\lambda\, d\phi\, d\theta} \quad (3)$$

where $I_{b\lambda}$ is the blackbody intensity given by Planck's formula. Although the formulae for the solar absorptance and the thermal emittance look very similar, the fact that the solar intensity and the blackbody intensity for moderate-temperature surfaces are distributed over different wavelength regimes (Fig. 3) can be utilized to design selective absorbers. By having a large emittance in the solar wavelengths and a small emittance in the infrared, absorbers can have high solar absorptance and low thermal emittance, thus resulting in a high absorber efficiency. Using spectrally-selective surfaces as solar absorbers was first proposed by Tabor in 1955[11]. A similar strategy can be pursued to take advantage of the differences in angular distribution between the solar spectrum and the (isotropic) blackbody spectrum[12], but that concept is relatively new and will not be discussed in this work.

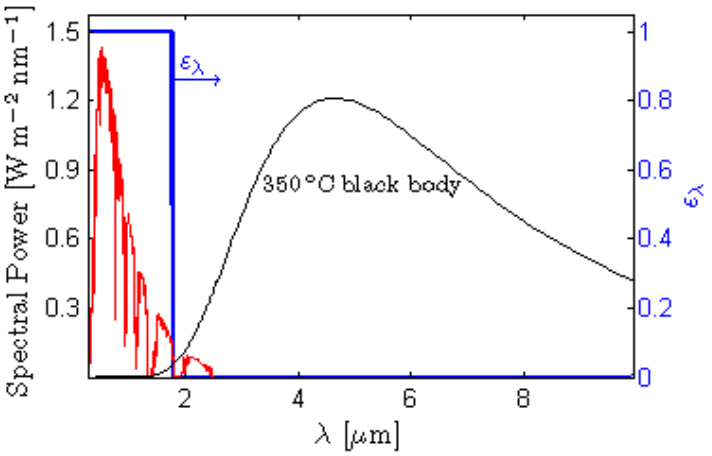

Fig. 3. Unconcentrated AM 1.5 Direct + Circumsolar spectrum (red, left axes) and spectrum of 350 ℃ blackbody (black, left axes). The ideal emittance profile (blue, right axes) transitions from 1 to 0 where the spectra cross, in this case at 1.8 μm

An ideal spectrally-selective absorber has an emittance of 1 at short wavelengths and 0 at long wavelengths, with a sharp transition between the two regimes. The wavelength where the transition occurs, λ_t, should be where the blackbody intensity begins to exceed the solar intensity[13] (Fig. 3). As represented in Fig, 3, the spectral intensity of a 350 ℃ blackbody exceeds the AM1.5 Direct + Circumsolar solar spectrum beginning at 1.8 μm. For higher-temperature absorbers, the ideal transition wavelength will shift to shorter wavelengths; at higher concentrations, the ideal transition wavelength will shift to longer wavelengths. The ideal transition wavelength is a function of both concentration and temperature (Fig. 4). The ideal transition wavelength is not a smooth function of temperature because the solar spectrum is not a smooth function; the crossover point will not occur at wavelengths where the solar spectrum is essentially zero due to atmospheric absorption. For space-based applications outside of the earth's atmosphere, these gaps would not exist; the optimal transition wavelength would be a smooth function of the hot-side temperature and the optical concentration.

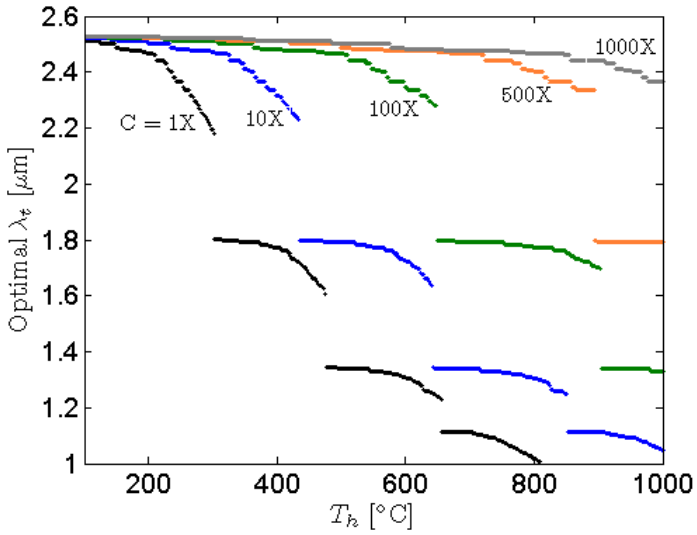

Fig. 4. Spectrally-selective absorber optimal transition wavelength as a function of hot-side temperature for five different optical concentrations[13]. The discrete jumps result from the fact that the solar spectrum reaching the earth drops to nearly zero around 1.4 μm and 1.8 μm (due to atmospheric absorption), and thus the blackbody spectrum cannot intersect the solar spectrum in these regions.

The ideal emittance profile drops from 1 to 0 at the transition wavelength. However, it is more realistic to assume that an emittance profile would drop down to a small but non-zero value after the transition wavelength. It is important to realize that this correction does not change the ideal transition wavelength in figure 4: the two spectra will cross at the same place regardless of the emittance profile. However, finite long-wavelength emittance does have a strong effect on the absorber efficiency as defined in equation (1). Even a long-wavelength emittance of only 0.01 drastically reduces the efficiency for high-temperature, low concentration applications. Because of this, the transition wavelengths that are worth investigating for terrestrial solar thermal applications are those between 1.6 and 1.8 μm, and between 2.2 and 2.5 μm.

While figure 4 gives a target transition wavelength for a spectrally-selective absorber for a given application (temperature and incident flux), it is also worthwhile to know the relative importance of the solar absorptance and thermal emittance on the absorber efficiency when evaluating real spectrally-selective absorbers. If the surface is enclosed in a vacuum, the convective

losses go to zero and the last term in the absorber efficiency equation (Eq. (1)) disappears. This equation can then be simplified as:

$$\eta_{abs} = \frac{q_h}{H_{abs}} = \alpha_s - w\varepsilon_t \tag{4}$$

where *w*, the weighting factor between the solar absorptance and thermal emittance, is:

$$w = \frac{\sigma_{sb}\left(T_h^4 - T_{amb}^4\right)}{H_{abs}} \tag{5}$$

When *w* is close to 1, the solar absorptance and thermal emittance are equally important for absorber efficiency. When *w* is much less than 1, the solar absorptance is the critical parameter. The weighting factor as a function of incident flux is plotted in Fig. 5. A typical domestic hot water heater operates near 1 kW/m^2 (1 sun) at a temperature near 100 ℃; this yields a weighting factor of 0.7, which indicates that the thermal emittance is nearly as important as the solar absorptance. A linear fresnel CSP plant operating at 60 suns and 350 ℃ has a weighting factor of 0.14, showing that an increase in solar absorptance of 0.01 produces a gain in efficiency equivalent to a reduction of thermal emittance of 0.07. Stirling-based parabolic dish CSP systems can reach fluxes exceeding 1000 kW/m^2 with operating temperatures reaching 700 ℃. Under such conditions, the weighting factor is less than 0.05, showing that solar absorptance is the critical parameter to improve. The benefit of knowing the weighting factor for a given application is that it allows for rapid calculation of the absorber efficiency, which is the best metric for absorber thermal performance.

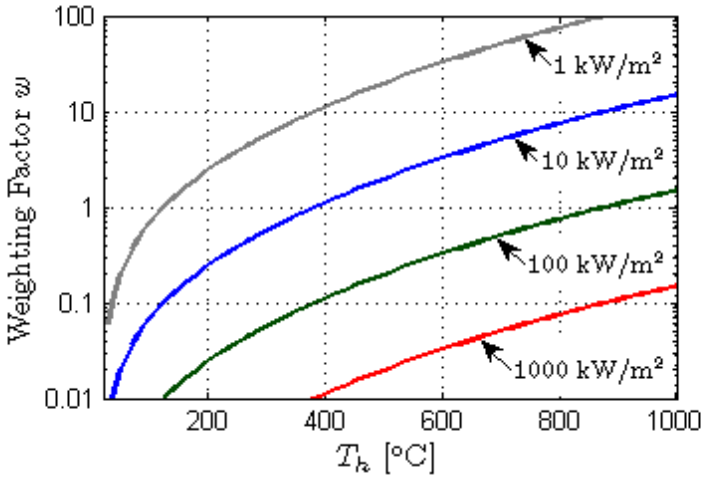

Fig. 5. The weighting factor as a function of surface temperature for four different incident solar fluxes. When the weighting factor is small, the absorber efficiency is most heavily influenced by the solar absorptance.

With this knowledge of the ideal transition wavelength as well as the relative importance of the solar absorptance versus the thermal emittance, we will review progress since 1955 on developing spectrally-selective absorbers.

Since the first studies on spectrally-selective coatings by Tabor and Gier in 1955 and after[14-16], investigations of various spectrally-selective absorbers have been carried out, such as black chrome coatings prepared by electrodeposition for solar hot water applications[17-20], Ni-Al_2O_3 cermet-based coatings prepared by sputtering and solution-chemical methods[21-23], $Cr/Cr_xO_y/Cr_2O_3$ multilayer absorber coatings[24], thickness-sensitive spectrally selective (TSSS) paints including organic black carbon and inorganic $FeMnCuO_x$ pigment[25], and thickness-insensitive spectrally selective (TISS) paints[26, 27]. Based on the configuration of coatings and the absorption mechanism, these spectrally-selective absorbers can be classified into six types[9]: 1) intrinsically selective, 2) semiconductor-on-metal coatings, 3) multilayer stacks, 4) metal-dielectric (cermet) composites, 5) textured surfaces, and 6) selectively-transmitting coatings on blackbody-like absorbers. However, in practical absorbers not just one but several mechanisms are invoked to achieve better spectral selectivity, such as multilayer cermet-based absorbers which comprise multilayer stacks and metal-dielectric composite coatings.

Cermet coatings have been extensively investigated and are now still extensively researched due to their high solar absorptance, low IR emittance, and good thermal stability for mid- and high-temperature applications such as concentrated solar power (CSP) systems and solar thermoelectric generators (STEGs). A cermet is a metal-dielectric composite in which metal is embedded in the dielectric matrix of an oxide, nitride, or oxynitride. A cermet should have ceramic characteristics in the visible spectrum and metallic properties in the IR. The coating thickness, constituents, and metal volume fraction in the matrix, as well as particle size, shape and orientation can affect how strongly the ceramic or metallic characteristics are expressed across the solar and IR spectra. Thicker coatings and smaller particle sizes are beneficial for high absorptance in the visible range. With an increase in particle radius, there is a shift of the visible absorption and scattering, resulting in lower

absorption. Thermal emittance in the IR can be decreased by decreasing the coating thickness and increasing the metallic concentration.[28]

Though some researchers have reviewed the process of mid- and high-temperature solar selective absorber materials and physical vapor deposited (PVD) spectrally-selective coatings for mid- and high-temperature solar thermal applications[9, 29], there are few reports focused on cermet-based spectrally-selective solar absorbers. Herein we present a detailed overview of cermet-based spectrally-selective coatings and treatments. We discuss one by one the solar thermal performance of different dielectric materials such as Cr_2O_3, Al_2O_3, AlN, SiO_2, and other materials, and give an outlook for cermet-based spectrally-selective absorbers.

3. Preparation of cermet-based solar absorbers

Many methods such as electroplating, anodization, physical and chemical vapor deposition and solution-based fabrication have been utilized to prepare cermet-based spectrally-selective absorbers.

3.1. Electroplating

Electroplating is an electrolytic process in which a metal anode goes into an electrolyte as it is deposited on cathode. Electroplating has been employed to prepare cermet spectrally-selective absorbers, especially black chrome comprising 75 percent chromium and 25 percent chromium oxide, which has been utilized in mid-temperature (~300 ^oC) parabolic trough solar collector systems[30, 31]. During the deposition process, the plating current density, bath temperature, substrate, and plating time can affect the morphology and performance of the as-prepared film. There are still some issues about nonuniform film thickness, high thermal emittance, and the environmental concerns of electroplating.

3.2. Anodizing

Similar to electroplating, anodizing also employs an electrochemical reaction in a special electrolyte to produce a coating. It was first utilized to protect seaplane parts from corrosion. Anodizing of aluminum is done in a suitable electrolyte, such as an aqueous solution of sulfuric acid, and aluminum is used as the anode in which an electrolytic reaction of aluminum with oxygen generated from the electrolyte takes place, producing an Al_2O_3-based cermet. Titanium can also be

anodized; the result is a coating whose color is dependent on the thickness of the deposited film. For aluminum, the color can be tuned by changing the preparation parameters such as time, temperature, and current density[32, 33]. Metallic dopants can be added during the anodization process to change the properties of the cermet.

3.3. Evaporation

Cermet films can also be created by the condensation of an evaporated material onto the substrate. In the process of thermal evaporation, the heating of material is carried out by a resistive heater or an electron beam. Various Al_2O_3 cermets (Al-Al_2O_3, Co-Al_2O_3, Pt-Al_2O_3, Cr-Al_2O_3) and black chrome were developed using this technique[34-36].

3.4. Chemical vapor deposition (CVD)

In 1893, the first industrial exploitation of chemical vapor deposition was patented by de Lodyguine, who demonstrated a deposition of W onto carbon lamp filaments via the reaction of WCl_6 and H_2. CVD is the reaction of gaseous reactants on or near a substrate surface in a heated, lighted, or plasma-filled environment. It can also be used to deposit high-purity, high-performance films. Various kinds of materials, such as semiconductors (Si, Ge, $Si_{1-x}Ge_x$), dielectrics (Al_2O_3, SiC, TiN, ZrO_2), and metal (Pt, W, Au, Cu) films can be developed using CVD. It can also be utilized to prepare solar selective surfaces, for instance, W-based metal oxide coatings used as a black metal spectrally-selective absorbers[37, 38].

3.5. Sputtering

Sputtering is a physical vapor deposition technique wherein a target material surface is eroded by particle bombardment and then condenses on a substrate. Sputtering can be used for large-area deposition. Many industrial applications, such as the deposition of metal films, semiconductor films, and antireflection coatings for optical applications, have been achieved using sputtering. Spectrally-selective solar absorbers have also been extensively developed by sputtering. Cr-Cr_2O_3 cermets have been deposited by using Cr and Cr_2O_3 composite targets with radio frequency (RF) sputtering or using a single Cr target via reaction sputtering in Ar+O_2 gas flow[39, 40]. Zhang *et al*. has deposited W-AlN, Mo-AlN, and stainless steel (SS)-AlN cermets by two-target DC

sputtering[41, 42]. During the deposition of M-AlN cermet layers, both targets were run simultaneously in the mixture of Ar and N_2.

3.6. Solution-based method

Various nanomaterials and ceramics have been fabricated by employing solution-based methods for many decades. In recent years, some spectrally-selective solar absorbers have been prepared by this route. Compared with other techniques, such as evaporation, CVD, and sputtering, the simplicity and low cost of solution-based processing allow it to be a possible candidate for large-scale deposition of spectrally-selective coatings. The biggest challenge is the preparation of a uniform and stable precursor containing as-designed metal ions. Ni-Al_2O_3 cermet-based spectrally-selective coatings have been prepared in an aqueous solution with a chelating agent and a wetting agent[43]. Ni nanochains embedded in an Al_2O_3 matrix were synthesized by mixing the Ni nanochains (prepared by the reaction of Ni^{2+} with N_2H_4) with Al_2O_3 sol[44].

4. Spectral selectivity of cermet-based absorbers

Cermet-based spectrally-selective absorbers have potential for high-temperature applications (over 400 ^oC). The preparation parameters and selective characteristics are summarized in Table 1. We discuss and review the performance of each kind of cermet-based absorber according to the dielectrics used.

Table. 1. Cermet-based spectrally-selective absorbers, sorted by host matrix. SS is stainless steel. Duration and temperature of stability tests are listed when reported. When noted with an asterisk, thermal emittance is extrapolated from room-temperature emittance data instead of measured at temperature.

Matrix	Metal Inserts	Preparation	Substrate	Stability	Solar Absorptance	Thermal Emittance	Ref.
Cr_2O_3	Cr	Electroplating	Aluminum	---	0.868	0.088* ($121\ ^oC$)	20
	Cr	Electroplating	Copper	$300\ ^oC$	0.93	0.12 ($27\ ^oC$)	19
	Cr	Electroplating	Aluminum	$350\ ^oC$	0.98	0.2 ($27\ ^oC$)	45

	Cr	Electroplating	Nickel	300 °C	0.96	0.25~0.35* (300 °C)	17
	Cr	Sputtering	Stainless Steel	300 °C	0.92	0.08* (121 °C)	40
	Cr	Sputtering	Copper	---	0.90~0.94	0.04* (65 °C)	39
	Cr	Sputtering	Copper	---	0.94	0.06* (82 °C)	46
	Cr	Sputtering	Optical slide	---	0.92~0.96	0.05~0.08* (100 °C)	47
Al_2O_3	Ni	Anodizing	Aluminum	250 °C in air	0.90~0.96	0.06~0.46 (100 °C)	49
	Ni	Evaporation	Fused-quartz	500 °C in air	0.94	0.1 (estimated)	23
	Ni	Sputtering	Stainless Steel	500 °C in air	0.94	0.07* (100 °C)	22
	Ni	Solution-based method	Aluminum	---	0.93	0.04* (100 °C)	51
	Ni	Solution-based method	Aluminum	---	0.93	0.03* (100 °C)	52
	Ni	Solution-based method	Aluminum	300 °C in air	0.93	0.05* (100 °C)	43
	Co	Evaporation	Nickel	---	0.95	0.1 (100 °C)	35
	Ag	Sputtering	Copper	400 °C in vacuum	0.93	0.04~0.05* (82 °C)	55
	Mo	Sputtering	Stainless Steel	2h @ 800 °C in vacuum	0.92	0.19 (80 °C)	56
	Mo	Sputtering	Stainless Steel	1h @ 800 °C in vacuum	0.92	0.16 (80 °C)	57
	W	Sputtering	Stainless Steel	580 °C in vacuum	0.939	0.12* (400 °C)	58
	Pt	Evaporation	Quartz	---	0.98	0.36* (200 °C)	36
AlN	W	Sputtering	Glass	500 °C in vacuum	0.939	0.039 (27 °C)	60
	W	Sputtering	Glass	---	0.953	0.051* (80 °C)	41
	SS	Sputtering	Glass	500 °C in vacuum	0.933	0.025 (27 °C)	61
	SS	Sputtering	Glass	---	0.94~0.95	0.04~0.05 (27 °C)	66
	Al	Sputtering	Aluminum	---	0.96	---	68

	Al	Sputtering	Glass	---	0.92	0.06* (100 °C)	69
SiO_2	Cu	Evaporation	Glass	277 °C	0.93	0.05 (27 °C)	72
	Cu	Evaporation	Metal or Glass	---	0.911	0.0196* (50 °C)	34
	Ni	Evaporation	Quartz	500 °C in vacuum	0.9	0.07 (100 °C)	73
	Ni	Sputtering	Aluminum	---	0.96	0.14* (100 °C)	75
	Au	Evaporation	Glass	---	0.88±0.01	0.014±0.005 (100 °C)	74
	Mo	Sputtering	Stainless Steel	580 °C in vacuum	0.94	0.13* (580 °C)	71
	Mo	Sputtering	Quartz	2h @ 800 °C in vacuum	0.95	0.075* (80 °C)	70
Other			Galvanized Iron	50h cycling 100-200 °C	0.93	0.08* (100 °C)	
NiS-ZnS	Ni/Zn	Solution-based method	Zincated Aluminium	24h cycling 100-200 °C	0.9	0.14* (100 °C)	76
			Zinc Electroplated Aluminium	50h cycling 100-200 °C	0.94	0.1* (100 °C)	
MoO_3	Mo	Solution-based method	galvanized steel sheet/zinc-plated mild steel sheet	300h 250 °C in air	0.88	0.2 (100 °C)	77
ZrO_2	Zr	Sputtering	Glass	---	0.97	0.05* (80 °C)	78
SS-N	SS	Sputtering	Glass	---	0.91	0.06* (82 °C)	79
HfMoN	Hf/Mo	Sputtering	Stainless Steel	200h @ 650 °C in vacuum 34h @ 475 °C in air	0.94~0.95	0.13~0.14* (82 °C)	80

4.1. Cr_2O_3-based cermets

Black chrome, a complex graded Cr-Cr_2O_3 composite on an Al or Ni substrate, can be produced by electroplating. McDonald has prepared electroplated black chrome on a 2 ft x 4 ft collector tube sheet[20]. The absorptance based on the air mass 2 spectrum (AM 2) and emittance based on the 121 ^oC blackbody spectrum are 0.868 and 0.088, respectively. The microstructure and thermal stability of black chrome have also been surveyed. Lampert and Washburn investigated the chemical and microstructural stability of black chrome at different temperatures and atmospheres[19]. There was little change on the microstructure and optical performance when annealed below 300 ^oC for a short term. A microcrystalline Cr_2O_3 phase was found after annealing at over 400 ^oC, and when the temperature increased to 500 ^oC, a new phase Cr_3O_4 appeared. An appreciable degradation of the optical performance was not observed up to 300 ^oC; a mild degradation was found near 400 ^oC. Major degradation appeared between 500 ^oC and 600 ^oC. The thermal stability of the coatings after long-term annealing (134 hours) at 350 ^oC in air was tested by Ritchie *et al*. on electroplated black chrome[45]. To further optimize the thermal stability of electrodeposited black chrome, Pettit *et al*. carried out a series of experiments through changing the bath composition (chromic acid, acetic acid, trivalent chromium and iron), substrate, plating current density, time, and temperature[17]. The most stable coatings were achieved with lower concentrations of trivalent chromium and additional agents. The solar absorptance should be stable at 0.96 for years of operation at 300 ^oC in air, when suitable techniques are applied.

Besides electroplating, physical vapor deposition has also been employed to prepare Cr_2O_3-based spectrally-selective cermets. Fan *et al*. deposited absorbers with a Cr/Cr-Cr_2O_3/Cr_2O_3 three-layer structure with a solar absorptance of 0.92 and a thermal emittance of 0.08. A co-sputtering technique was applied in the deposition process of the Cr-Cr_2O_3 cermet layer, which resulted in a similar optical performance compared to the electroplated black chrome[40]. Cermets can also be deposited using reactive sputtering with direct current (DC) power. Much work associated with Cr_2O_3 cermet-based spectrally-selective absorbers has been done. Teixeira *et al*. prepared graded layers of Cr-Cr_2O_3 on Cu substrates by varying the oxygen gas flow and achieved absorbers with solar absorptances in the range of 0.90 to 0.94 and thermal emittances of 0.04[39]. Further optimization of the graded cermet film structure was carried out by Nunes *et al*.[46]. They proposed the configuration of four-layer coatings consisting of one anti-reflection layer on top of three cermet layers in which the Cr metal fraction decreases from substrate to surface. A solar aborptance of 0.94 and a thermal emittance of 0.06 at 82 ^oC were obtained. Yin *et al*. developed another film structure

with an LHL configuration (L: low metal volume fraction in cermet, H: high metal volume fraction in cermet) made by changing the target current[47]. The absorber deposited on an optical slide coated with 200 ~ 400 nm of chromium had a solar absorptance in the range of 0.92 ~ 0.96 and a thermal emittance between 0.05 and 0.08 at 100 ^{o}C. The stability of coatings upon annealing at 170 ^{o}C for a long time (840 days) indicated it was suitable for solar hot water applications. As shown in Fig. 7, the reflection spectra after annealing at 200 ^{o}C, 300 ^{o}C, 400 ^{o}C and 500 ^{o}C in vacuum for 1 hour demonstrated the coatings were thermally stable up to 300 to 400 ^{o}C. As for the preparation on a large scale, Graf *et al*. prepared sputtered solar absorber coatings (~ 60 m^2) on copper sheets based on chromium oxynitride by using DC-magnetron sputtering[48]. The absorbers showed good optical properties with $\alpha_s > 0.93$ and $\varepsilon_t < 0.07$ at 100 ^{o}C.

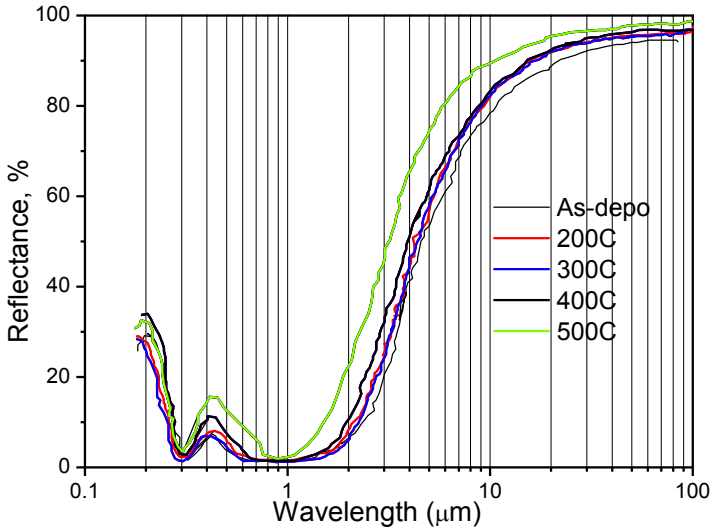

Fig. 7. Reflectance spectra of an LHL profile Cr-Cr_2O_3 cermet spectrally-selective coating on an optical slide coated with 200 ~ 400 nm of chromium, after treatment under different annealing temperatures. Reprinted from ref. 47 with permission.

Figure 8 summarizes the spectral selectivity of black chrome produced through electroplating and physical vapor deposition. The highest solar absorptance of surfaces obtained from those different methods is almost the same, however high thermal emittance cannot be avoided on the coatings prepared by electroplating. Although the cost of electroplating is low, the environmental issues caused by electroplating should result in it being replaced by another manufacturing method in the future.

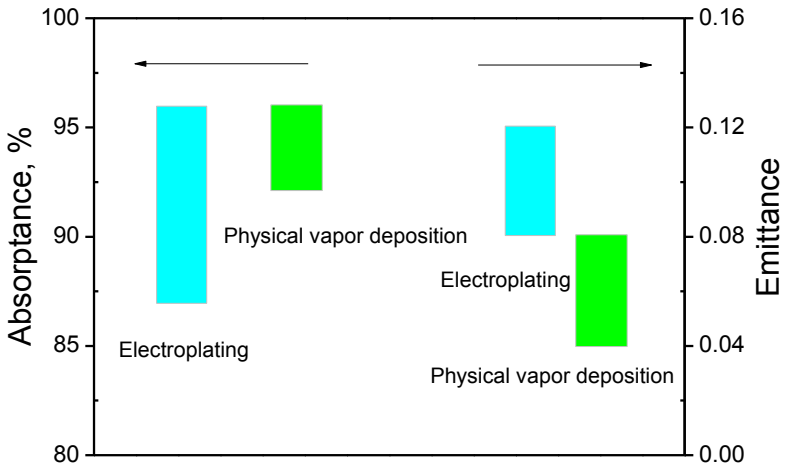

Fig. 8. The comparison of solar absorptance and thermal emittance of black chrome prepared by electroplating[17, 19, 20] and physical vapor deposition[39, 40, 46, 47]. The emittance was obtained at 82 ^{o}C or 100 ^{o}C.

4.2. Al_2O_3-based cermets

Al_2O_3-based cermet coatings which have excellent optical properties and thermal stabilities have been extensively investigated as spectrally-selective absorbers. Nickel-pigmented anodized aluminum (Ni particles embedded in anodized aluminum) was prepared by Kumar *et al*. by anodizing Al sheets or foil, followed by electrolysis in a Watt's type of nickel electroplating bath with a thick Ni sheet as a counter electrode[49]. They also studied the correlation of anodizing parameters with spectral selectivity. The solar absorptance and thermal emittance can be varied by adjusting the anodizing parameters, such as the bath temperature, anodization voltage, anodization time, and the concentration of H_2SO_4 and H_3PO_4. To improve the corrosion resistance of those solar absorbers, Moller *et al*. developed a hydrophobic post treatment method[50], which seemed to be a promising alternative to replace the other sealing methods for spectrally-selective absorber surfaces. Other techniques, such as, co-evaporation, reactive sputtering, and solution based methods, were also employed to prepare Ni-Al_2O_3 cermet-based solar selective surfaces. Craighead *et al*. investigated the spectral selectivity of a Ni-Al_2O_3 cermet deposited by duel-electron-beam evaporation and a high solar absorptance of 0.94 at air mass 2 was achieved[23]. RF magnetron sputtering was used to prepare Ni-Al_2O_3 cermet films by Sathiaraj *et al* [21, 22]. The metal fractions of the cermet layers were varied by using targets with different compositions and by co-sputtering the

target with additional nickel pellets arranged along the magnetron ring. The reflection spectra of the Ni-Al_2O_3 cermet layer (65 nm thick) with and without a SiO_2 anti-reflection layer are shown in Fig. 9. The solar absorptance of 0.94 and thermal emittance of 0.07 at 100 ^oC were calculated from the reflectance curve in Fig. 9. The Ni-Al_2O_3 coating deposited on the molybdenum-coated nickel-plated stainless steel with a protective SiO_2 coating as an anti-reflection layer was stable up to 500 ^oC in air.

Solution-chemical methods were also developed to prepare the selective solar absorbers. Boström *et al*. employed a promising novel solution-based method to synthesize Ni-Al_2O_3 cermet-based coatings on aluminum substrates[51]. The optimal coating, with a nickel content of 65%, a thickness of 0.1 μm, and particle size of ~ 10 nm has a normal solar absorptance of 0.83 and a normal thermal emittance of 0.03 at 100 ^oC. To further optimize the spectral selectivity, an anti-reflection layer was added with a sol-gel process. The silica, hybrid silica or alumina AR film was obtained after annealing the coatings at 580 ^oC[52]. The optimized sample was achieved when alumina was used as an AR coating; the absorber had a solar absorptance of 0.93 and a thermal emittance of 0.03 at 100 ^oC. The structure and morphology of nickel-alumina/silica spectrally-selective absorbers were investigated by Boström *et al.*[53]. The size of the Ni metal particles dispersed in the Al_2O_3 was in the range of 3-10 nm, which is small enough compared with the wavelengths of interest. Micro-cracking can be avoided by using hybrid silica compared with pure silica. Ni-Al_2O_3 coatings prepared via an aqueous solution-chemical method was suggested by Li *et al.*[43]. In the process of preparation, the aqueous solution had many advantages, such as its abundance, lower cost, and low toxicity. They found that a single Ni-Al_2O_3 coating on an aluminum substrate demonstrated a high normal solar absorptance of 0.85 and a low thermal emittance of 0.03 at 100 ^oC, and a three-layer coating consisting of a double absorption layer and one anti-reflection layer indicated a better selectivity with a solar absorptance of 0.93 and a thermal emittance of 0.05 at 100 ^oC. The thermal stability of the three-layer coating was evaluated in air at 250 ^oC and 300 ^oC, as shown in Fig. 10, which indicated it was stable in air up to 300 ^oC. Wang *et al*. observed that surface plasmon polaritons enhanced solar absorption in a Ni nanochain-Al_2O_3 cermet structure, which demonstrated a high solar absorptance exceeding 0.90 and low thermal emittance of less than 0.10[44]. The authors also discovered that the spectral selectivity can be tailored by changing the length of Ni nanochains.

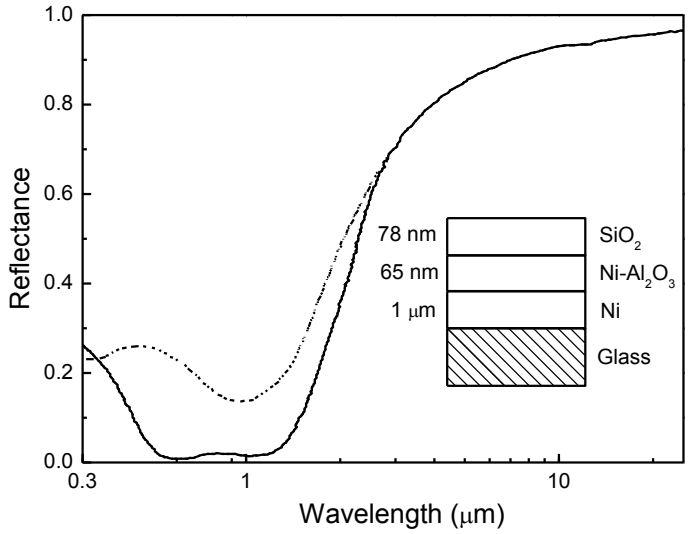

Fig. 9. The reflectance spectra of a 65 nm Ni-Al_2O_3 film (dashed line) and after overcoating with 78 nm of SiO_2 (solid line). Reprinted from ref. 22 with permission.

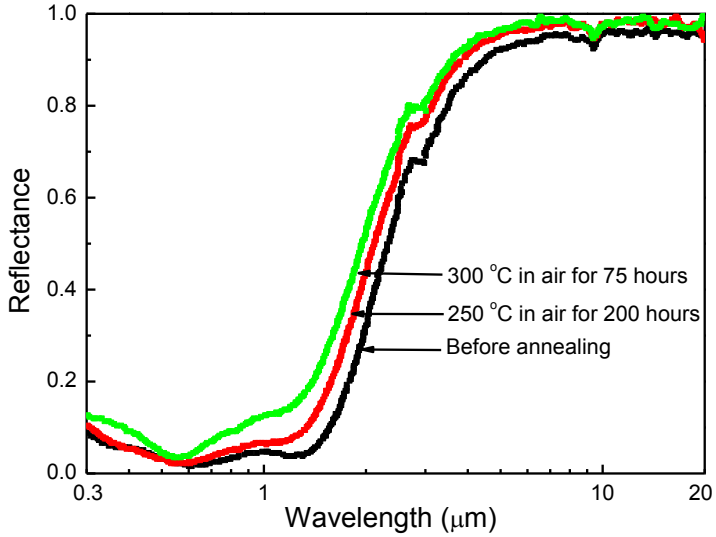

Fig. 10. Thermal stability of three-layer sample $Ni_{90}Al_{10}/Ni_{40}/Al_{60}/SiO_2$ in air after annealing at 250 ^oC and 300 ^oC, respectively. Reprinted from ref. 43 with permission.

Besides Ni, other metals such as Ag, Co, Ti, Mo, W, and Pt were also used as inclusions in an Al_2O_3 matrix. Niklasson *et al*. prepared Co-Al_2O_3 cermet films by vacuum co-evaporation of Co

and Al_2O_3[35]. The optimized absorber, with a 70 nm Co-Al_2O_3 (58 vol% Co) cermet layer and a 70 nm Al_2O_3 anti-reflection layer on Corning 7059 glass coated with an opaque Ni layer, had a solar absorptance of 0.95 and a thermal emittance of near 0.10 at 100 ^oC. Titanium – a lightweight metal with good corrosion resistance – was embedded in Al_2O_3 dielectric materials through pulsed laser deposition by Chen *et al.*[54]. The extinction coefficient increased and the real part of the refractive index decreased with increasing Ti content in the UV and visible wavelength range. The two-layer Ti-Al_2O_3 film demonstrated promising spectral selectivity. Ag-Al_2O_3 cermet films on copper, silicon and glass were also prepared with an unbalanced magnetron sputtering technique. A broad absorption peak was observed at ~ 610 nm, which was due to the surface plasmon resonance of Ag nanoparticles embedded in the Al_2O_3 matrix[55]. This structure exhibited a high solar absorptance (0.93) and low thermal emittance (0.04~0.05) at 82 ^oC. There was no shift of Raman peaks in the coatings upon annealing for 2 hours in vacuum at 400 ^oC. Mo was also investigated as a metal addition in Al_2O_3 cermets. Graded Mo-Al_2O_3 cermet coatings on Al or Cu substrates were produced by gradually adjusting the oxygen gas flow during reactive sputtering by Teixeira *et al.*[39]. Those coatings demonstrated a good spectral selectivity with a solar absorptance of 0.88 - 0.94 and a thermal emittance of 0.09 - 0.15. The microstructure and spectral selectivity of a series of films including Mo, Al_2O_3, Mo/Al_2O_3 tandems, and Mo-Al_2O_3 multilayers deposited on stainless steel via magnetron sputtering were investigated[56]. The optimized absorber, with double Mo/Al_2O_3 cermet layers and one Al_2O_3 anti-reflection layer, had a solar absorptance of 0.92 and thermal emittance of 0.19 at 80 ^oC. After annealing at 800 ^oC for 2 hours in vacuum, the solar absorptance decreased to 0.91 and the thermal emittance increased to 0.27. There were some defects, such as widened boundaries and cracks and holes in the Al_2O_3 layer after high temperature treatment (> 650 ^oC), which could induce the Mo diffusion and deteriorate the spectral selectivity of the coatings. The improved thermal stability of Mo-Al_2O_3 cermet-based spectrally-selective absorbers was achieved by Cheng *et al*. using a similar preparation procedure as Du's work[57]. The stability of W embedded in an Al_2O_3 matrix prepared by co-sputtering was investigated by Antonaia *et al.*[58]. There was a slight change in the reflectance spectrum upon annealing at 580 ^oC for 2 days in vacuum, but thermo-mechanical degradation, such as fracturing, peeling, and adhesion, did not appear. The stability of each layer, investigated with FTIR and XRD data, indicated that the tungsten metal back reflector underwent a phase transition from β to α; tungsten in Al_2O_3 was partially oxidized; and the amorphous Al_2O_3 tended to form the γ phase upon annealing. For higher temperature applications

(up to 650 ^{o}C), noble metals were chosen as the inclusions in the dielectric matrix due to their chemical inertness and stability. Graded Pt-Al_2O_3 composites were also prepared through the co-evaporation of Pt and Al_2O_3 and a textured SiO_2 layer was obtained by etching with a plasma of CF_4 gas. With the help of the textured SiO_2 anti-reflection layer, the solar absorptivity of this graded coating was as high as 0.98[36]. Nuru *et al*. prepared Pt-Al_2O_3 on a Mo-coated stainless steel substrate using radio-frequency sputtering[59]. The XRD indicated that the Al_2O_3 matrix was fully amorphous, and the size of the Pt inclusions was about 3.2-4.7 nm using the Debye-Scherer approximation, which is consistent with the results obtained from SEM and AFM. An absorptance exceeding 0.98 can be achieved across the UV/visible/near IR range.

The solar absorptance and thermal emittance of the typical Al_2O_3-based cermet absorbers with different metal inclusions (Ag, Co, Mo, Ni, Pt, and W) are summarized in Fig. 11. Although the IR reflector layer or substrate has a large effect on the thermal emittance, the metal inclusions, especially in the bottom layer adjacent to the substrate or IR reflector layer, also affect the thermal emittance due to the similar metal characteristics in this layer. Among those metal inclusions, the surface based on Ag embedded in Al_2O_3 demonstrates a low thermal emittance at 82 ^{o}C. The solar absorbers which had a W-Al_2O_3 absorption layer showed a thermal emittance of 0.1 at 400 ^{o}C, which is promising for CSP applications. Ni-Al_2O_3 cermet-based absorbers, marked by the ellipse in Fig. 11, display different emittances ascribed to different preparation techniques. A high thermal emittance of 0.1 - 0.2 was found in the absorber prepared by electrochemical deposition. Physical deposition and solution–chemical methods can result in low thermal emittances. The absorptances of those surfaces were in the range of 0.88 ~ 0.98. The highest was obtained with a Pt-Al_2O_3 absorber.

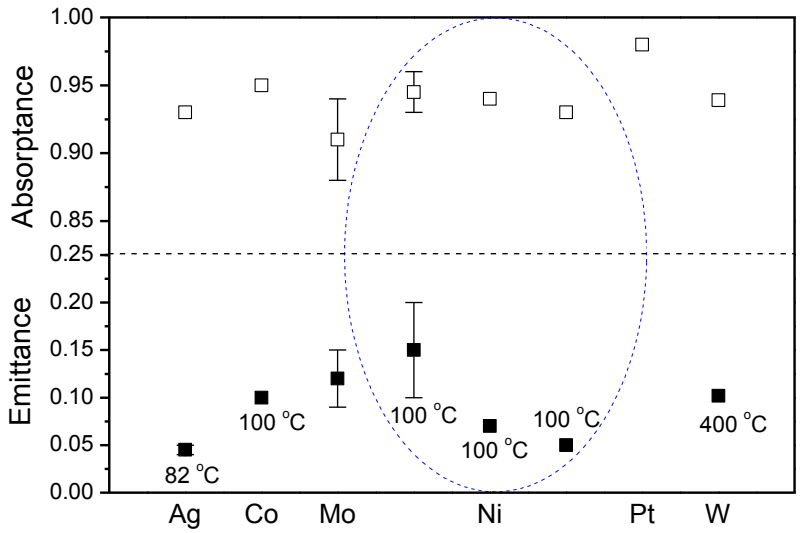

Fig. 11. The solar absorptance and thermal emittance of spectrally-selective absorbers with different metals (Ag, Co, Mo, Ni, Pt and W) embedded in an Al_2O_3 matrix[22, 33, 35, 36, 39, 43, 55, 58].

4.3. AlN-based cermets

Aluminum nitride, which has high thermal and chemical stability, was chosen as a dielectric for some cermets. Zhang *et al*. carried out extensive work on AlN-based cermets for absorber coatings[41, 42, 60-66]. W-AlN cermets were prepared by simultaneous deposition of Al and W in a gas mixture of argon and nitrogen. Due to the high chemical reactivity of aluminum with nitrogen and the excellent nitriding resistance of tungsten metal, AlN dielectrics with tungsten inclusions can be achieved using DC reactive sputtering. As shown in Fig. 12, the reflectance spectra of the absorbers with double cermet layers and one AlN anti-reflection layer on an Al IR reflector coated substrate indicated a solar absorption of 0.939 and a normal thermal emittance of 0.039 at room temperature[60]. The film, after baking at 500 ^{o}C in vacuum, demonstrated a nearly identical emittance as that of a pristine film. Calculations based on a modified Bruggeman method[67] to optimize the films were carried out by Zhang[41]. Three-layer and four-layer cermet coatings based on the calculations demonstrated similar spectrally-selective characteristics. The optimized coatings with film structures of AlN/W-AlN (low metal volume fraction (LMVF) /W-AlN (high metal volume fraction (HMVF) /Al have a high solar absorptance of 0.953 and a near-normal emittance of 0.051 at 80 ^{o}C under 2X optical concentration. Similar to a pure AlN dielectric, the LMVF cermet was transparent in the IR and therefore had a similar thermal emittance. The HMVF cermet with the metal filling factor of 0.56-0.58 had metal-like characteristics and had a large effect on the emittance of the

structure. In these HMVF cermets, the contribution of the IR reflector layer (W, Cu or Al) on the emittance can be ignored. Since stainless steel (SS) has excellent nitriding resistance, it can be used as metal component in AlN-based cermets. When depositing AlN via reactive sputtering of Al with nitrogen, there is a sharp transition from the metal mode to the dielectric mode depending on the nitrogen partial pressure[61]. It is reasonable to adjust the composition of SS-AlN cermet by changing the deposition time ratio of SS to AlN. The design of double cermet structures was also employed in this system. The reflectance spectrum can be shifted by changing the thickness of each layer. Reducing the thickness of the HMVF cermet layer from 64 nm to 53 nm induced a shift towards shorter wavelengths. Increasing the thickness of the LMVF cermet layer from 16 nm to 32 nm resulted in a shift towards longer wavelengths. The thermal stability of the sample with the configuration of AlN (70 nm)/SS-AlN(LMVF) (16 nm)/SS-AlN(HMVF) (53 nm) was inspected and is shown in Fig. 13. There was a slight change in the reflectance spectrum after baking at 500 ^{o}C for 1 hour in vacuum, which resulted in an increase in solar absorptance from 0.933 to 0.937 and an increase in thermal emittance from 0.025 to 0.029 at 20 ^{o}C. A commercial-scale cylindrical DC magnetron sputter coater was developed by Zhang *et al*. in 1998[66], which can be used to deposit metal-aluminum nitride cermet coatings on glass tubes. The chamber can accommodate thirty-two glass tubes with outside diameters of 37 mm and lengths of 1.2 m. Zhao *et al*. prepared Al-AlN cermets through the reactive sputtering of Al with nitrogen gas[68]. The different composites of Al-AlN cermets can be tuned by changing the nitrogen gas flow during the process of sputtering. The optical parameters of the cermets were determined using a dielectric function model of the two constituents in Bruggeman's equation. The high solar absorptance of 0.97 can be predicted by modeling the film structure as two graded absorption layers and an anti-reflection layer. The optimized solar absorber demonstrated a high solar absorptance of 0.96. The design of a textured surface was applied in the Al-N system. Different surface roughnesses of sputtered Al films were achieved through a method of two-step deposition of the Al film with different substrate temperatures[69]. With increasing the substrate temperature of the lower reflector layer, the surface roughness increases. Compared with the flat film, a surface with suitable roughness can improve the solar absorptance without increasing the thermal emittance.

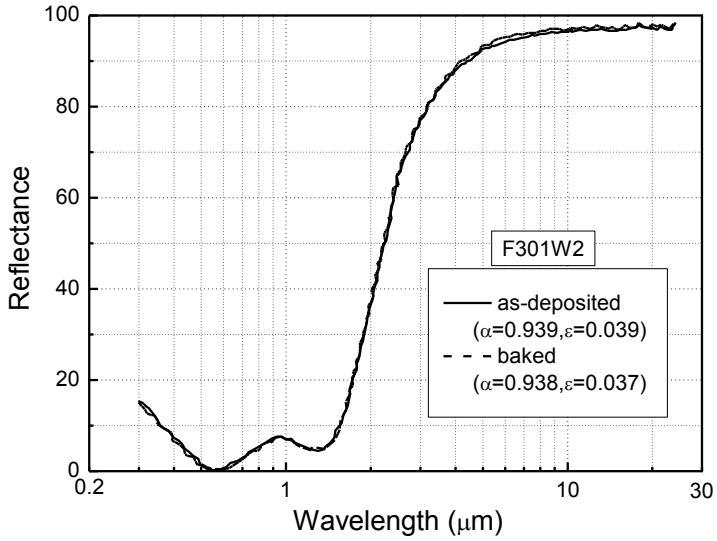

Fig. 12. The near normal reflectance spectra of sample F301W2 with the structure of AlN/W-AlN(LMVF)/W-AlN(HMVF)/Al. The solid line is as-deposited; the dashed line is after baking in vacuum at 500 ^{o}C for 1 hour. Reprinted from ref. 61 with permission.

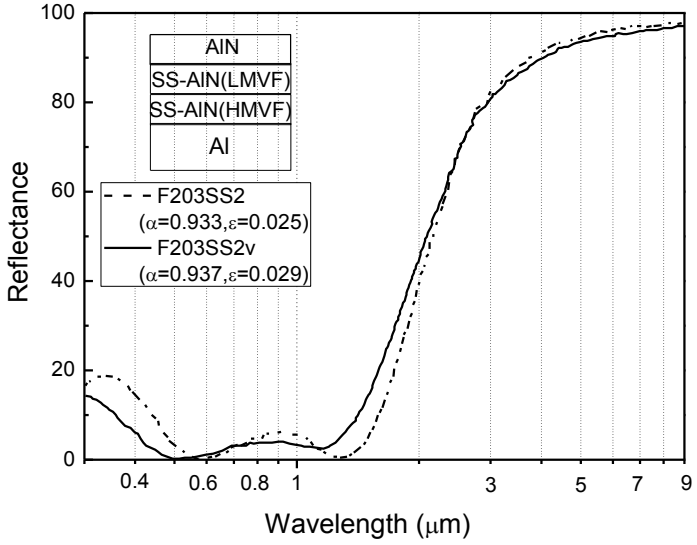

Fig. 13. The reflectance spectrum of F203SS2 baked in vacuum at 500 ^{o}C for 1 hour (solid curve). As a comparison, the reflectance spectrum of the as-deposited film is also included (dashed curve). Reprinted from ref. 61 with permission.

4.4. SiO_2-based cermets

Amorphous silicon dioxide was long used as anti-reflection layer. It can be utilized in cermets as the dielectric material due to its high chemical and thermal stability. The metals Cu, Ag, Au, Ni and Mo embedded in SiO_2 media have been investigated as spectrally-selective coatings[70-74]. Cu-SiO_2 cermets prepared by simultaneous evaporation of silicon dioxide and copper with an electron beam heater and electric-resistance heater, respectively, were used as absorption layer for spectrally-selective absorbers by Garnich *et al.*[72]. The filling factor of metal in the dielectric matrix and the thickness of the cermets can directly determine the spectral selectivity of the coatings. The transition wavelength can be adjusted by changing the filling factor and thickness of the cermet layer. With the optimum thickness (50-200 nm) and filling factor (20% - 40%) of the cermet, the transition wavelength can shift to shorter wavelengths with decreasing thickness and filling factor of the cermet layer. Cu-SiO_2/Cu tandems showed large degradation upon tempering above 400 ^oC in vacuum due to Cu diffusion. Structures comprising double absorption layers of HMVF and LMVF were employed in the Cu-SiO_2 system. Zhang *et al*. deposited double absorption layers of Cu-SiO_2 cermets by co-evaporation of Cu and SiO_2[34]. With the help of a SiO_2 anti-reflection layer, the absorber demonstrated a high solar absorptance of 0.911 and low normal thermal emittance of 0.0196 at 50 ^oC. To improve the thermal stability of SiO_2-based cermets, Okuyama *et al*. chose Ni as the inclusion[73]. The Ni-SiO_2 cermets were prepared by evaporation of a pressed mixture of Ni and SiO_2. The complex refractive index was calculated by fitting a model to the transmittance and reflectance data. The real part of the refractive index of the Ni-SiO_2 cermet was slightly larger than that of SiO_2. The coatings with 87 nm of Ni-SiO_2 cermet and 73 nm of SiO_2 demonstrated good optical properties with high absorptance in the visible and near-IR range and high reflectance in the IR range. A solar absorptance of 0.90 can be obtained with this absorber. The thermal emittance, which was measured by cooling the heated sample, increased with temperature. The thermal stability of the coatings was good; little spectral and mechanical degradation was found after treatment in a vacuum at 420 ^oC for 40 hours and at 515 ^oC for 12 hours. Farooq *et al*. utilized a co-sputtering technique to prepare Ni-SiO_2 cermets and studied the influence of substrate choice, film thickness, and film composition on spectral selectivity[75]. The solar absorptance of coatings deposited on bulk aluminum was 0.91. A larger absorptance (0.96) and also a larger thermal emittance were found when the coatings were deposited on Ni-coated Al. This increase is probably due to the rough surface of the Ni-coated Al. As shown in Fig. 14, the reflectance spectrum of the surface with thick Ni-SiO_2 composites is shifted to longer wavelengths compared to that with thin

Ni-SiO_2 composites. Gold was also embedded in a SiO_2 matrix via co-evaporation of Au and SiO_2 by electron beam evaporation[74]. The very low thermal emittance of 0.014 ± 0.005 at 100 ^oC was obtained from a thermal radiation experiment compared with the radiation of a black body. The optimization of Mo-SiO_2 spectrally-selective coatings was carried out by Esposito *et al*. through a semi-empirical procedure[71]. The complex index of refraction of each layer was estimated from ellipsometric measurements and was used to simulate the photo-thermal parameters. The optimized coatings on stainless steel demonstrated a very low thermal emittance of less than 0.13 and a solar absorptance of 0.94 was measured in vacuum at 580 ^oC. Further evaluation of the thermal stability of a Mo-SiO_2 selective surface was carried out at 754 ^oC[70]. There was little change of the XRD patterns of LMVF Mo-SiO_2/SiO_2 and HMVF Mo-SiO_2/SiO_2 after annealing at 754 ^oC for 2 hours in vacuum compared with the pristine ones, which indicated the Mo-SiO_2/SiO_2 tandem was still amorphous even after annealing. The cermet coating on quartz glass with a Mo IR reflector 150 nm thick showed a high absorptance of 0.95 and a low emittance of 0.075 at 80 ^oC upon annealing at 754 ^oC, and demonstrated a high thermal stability.

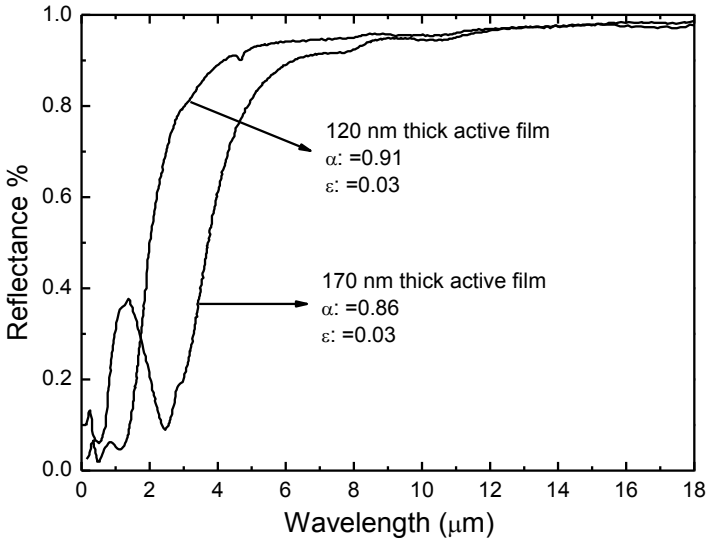

Fig. 14. The reflectance spectra of Ni-SiO_2 selective solar absorber coatings with different active film thicknesses. Reprinted from ref. 75 with permission.

The dependence of the spectral selectivity on the metal inclusions is depicted in Fig. 15. For the Cu, Au, Mo, and Ni/SiO_2 absorbers, the IR reflector material is the same metal as the inclusion. An emittance of less than 0.03 was achieved on the absorbers using Cu or Au as a reflector layer, which is reasonable due to the low emissivity of Cu and Au. Regarding the Ni-SiO_2 cermet

absorbers, the emittance of 0.03 was obtained with a bulk aluminum substrate; the high emittance of 0.14 was achieved with a Ni-coated Al substrate. The Mo-SiO_2 based absorber exhibited a low emittance even at 400 ^oC, indicating its potential for many mid-temperature applications. The Au-SiO_2 based cermet has the lowest solar absorptance and the lowest thermal emittance, indicating the highly reflectivity of Au plays a role across the entire spectrum.

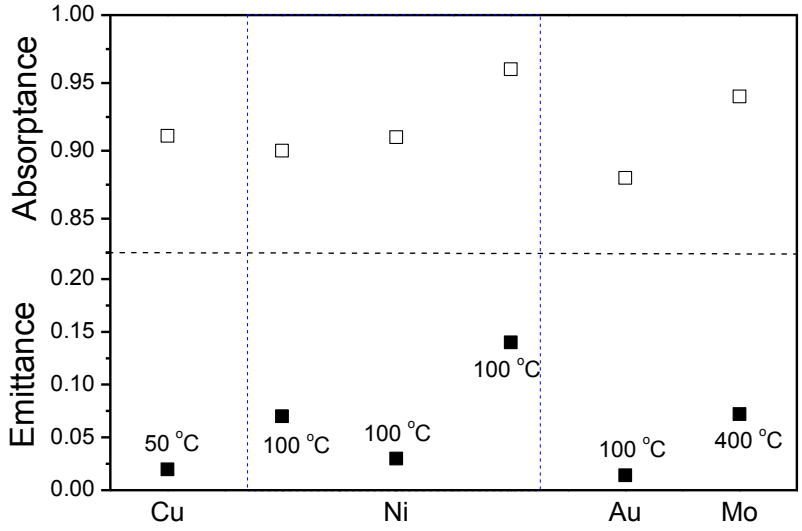

Fig. 15. The solar absorptance and thermal emittance of various spectrally-selective absorbers with different metals (Cu, Ni, Au, and Mo) embedded in an SiO_2 host[34, 71, 73-75].

4.5. Other cermets

Other composites such as black nickel and black molybdenum were developed for flat plate solar collectors. Gogna *et al*. utilized a chemical conversion technique to deposit black nickel coatings. Silmilar to black chrome, black nickel comprises nickel, zinc, nickel sulfide, and zinc sulfide[76]. The solar absorptance and thermal emittance of black nickel deposited on galvanized iron depended strongly on the dipping time at different bath temperatures and solution pH values. With increasing dipping time, the solar absorptance increased and reached a saturated value before decreasing again slightly. However, the thermal emittance increased gradually due to the increased thickness of black nickel. There was no effect on the coatings deposited on galvanized iron or zinc electroplated aluminum substrates after a 6-month outdoor exposure test. A similar simple, low-cost

technique was employed to prepare black molybdenum[77]. The optimized spectrally-selective absorbers had a solar absorptance of 0.88 and a thermal emittance of 0.2. Good thermal stability and high adhesion were found on the coatings deposited on galvanized steel sheet and zinc-plated mild steel sheet.

The Zr-ZrO_2 cermets deposited via DC reactive sputtering were used as spectrally-selective coatings for solar absorbers[78]. The optimization of the film configuration was carried out with a numerical model to maximize the absorber efficiency. The optimized film with the structure of Al_2O_3/Zr-ZrO_2 (LMVF)/Zr-ZrO_2 (HMVF)/Al demonstrated a high solar absorptance of 0.96, a normal thermal emittance of 0.05 at 80 ^oC, and good thermal stability at 300 to 350 ^oC in air. Using one stainless steel (SS) target, Juang *et al*. deposited SS/SS-N films by varying nitrogen gas flow ratios during deposition[79]. The HMVF SS/SS-N cermets could be obtained at a low nitrogen gas ratio. By increasing the nitrogen gas ratio to 15%, the cermet was gradually changed to LMVF. It evolved into a dielectric material when the nitrogen gas ratio exceeded 17.5%. The three-layer coatings comprising HMVF and LMVF cermet layers and a dielectric layer had a solar absorptance of 0.91 and a thermal emittance of 0.06 at 82 ^oC, which was close to the predicted value. To extend the application to higher temperatures, HfN- and MoN-based materials were explored as spectrally-selective coatings due to their high thermal stability and excellent optical characteristics.

A new HfMoN(HMVF)/HfMoN(LMVF)/HfON/Al_2O_3 tandem coating on a SS substrate was developed by Selvakumar *et al*. using reactive pulsed DC unbalanced magnetron sputtering[80]. Each layer was deposited using Hf, Mo and Al metallic targets under different gas ratios of Ar, N_2 and O_2. The four-layer tandem exhibited high thermal stability in vacuum at 600 ^oC for 450 hours, 650 ^oC for 100 hours and in air at 475 ^oC for 34 hours.

5. Outlook and Conclusion

For high-temperature CSP applications, achieving thermally-stable spectrally-selective absorbers remains a major challenge. One strategy is to explore new materials, including metal inclusions and dielectrics, which have high thermal stability and excellent optical properties for high temperature applications, especially above 500 ^oC. Stable oxide and nitride materials, such as Y_2O_3, ZrO_2, HfN and TiN, should be extensively investigated. Also, metal inclusions with high melting points and high nitriding and oxidation resistance, such as noble metals, should be an

interesting topic for cermet-based spectrally-selective absorbers. Besides choosing stable materials for coatings, avoiding the diffusion of metal at high temperatures is another issue. Pretreatment of stainless steel substrates in air to form oxide coatings can prevent the diffusion between the metallic IR reflector and the substrate[57]. To maximize the absorber efficiency, multiple absorption mechanisms should be employed. As for cermet-based absorbers, we should fully take into account the interference effect with different layers as well as the intrinsic absorption of each cermet layer in the design of multilayer films. Accurate information on the cermet optical constants over a wide wavelength range is needed for simulations of multilayer designs. Regarding the cermet layer, the solar absorption strongly depends on the uniform distribution and suitable size of the metal inclusions in the dielectric, the particle size orientation, the metal volume fraction, as well as other factors. To address degradation, it is necessary to investigate microstructure changes after long-duration annealing in air or in vacuum. In pursuit of high absorber efficiency, we should also consider cost and environmental issues. Solution-based methods can meet the requirement of low cost, however the coatings prepared by this method have a relatively low spectral selectivity compared with other techniques. The incorporation of a solution-based method with other techniques, such as CVD, evaporation, or sputtering may balance the cost and performance of the absorber.

In this article, we mainly focused on cermet-based spectrally-selective absorbers. State-of-the-art cermet materials prepared through various methods, such as electroplating, anodizing, evaporation, CVD, sputtering and solution-based methods, were reviewed based on the different dielectric materials in cermet. Absorbers incorporating cermet coatings based on Cr_2O_3, Al_2O_3, AlN, SiO_2, and other materials were introduced one by one and their spectral characteristics were analyzed. The spectral properties of the cermets can be changed by varying the experimental parameters and film configurations to maximize the absorber efficiency.

Acknowledgements

This work is supported by “Concentrated Solar Thermoelectric Power (CSP)” under award number DE-EE0005806.

Notes and references

1. P. M. Boffey, *Science*, 1970, **168**, 1554-1559.
2. D. Abbott, *P IEEE*, 2010, **98**, 42-66.
3. A. Shah, P. Torres, R. Tscharner, N. Wyrsch and H. Keppner, *Science*, 1999, **285**, 692-698.
4. G. Masson, M. Latour, M. Rekinger, I.-T. Theologitis and M. Papouts, in *European Photovoltaic Industry Association*, ed. C. Winneker, 2013.
5. D. Mills, *Sol Energy*, 2004, **76**, 19-31.
6. D. Kraemer, B. Poudel, H. P. Feng, J. C. Caylor, B. Yu, X. Yan, Y. Ma, X. W. Wang, D. Z. Wang, A. Muto, K. McEnaney, M. Chiesa, Z. F. Ren and G. Chen, *Nat Mater*, 2011, **10**, 532-538.
7. F. Mauthner and W. Weiss, in *Markets and Contribution to the Energy Supply 2011*, Solar Heating & Cooling Programme International Energy Agency, 2013.
8. N. Wang, L. Han, H. C. He, N. H. Park and K. Koumoto, *Energ Environ Sci*, 2011, **4**, 3676-3679.
9. C. E. Kennedy, National Renewable Energy Laboratory, 2002.
10. G. A. Niklasson and C. G. Granqvist, *J Mater Sci*, 1983, **18**, 3475-3534.
11. H. Tabor, in *Transactions of the Conference on the use of Solar Energy*, The Scientific Basis, October 31-November 1, Tucson, 1955.
12. P. Bermel, J. Lee, J. D. Joannopoulos, I. Celanovic and M. Soljacic, *Annual Review of Heat Transfer*, 2012, 14.
13. K. McEnaney, in *Department of Mechanical Engineering*, Massachusetts Institute of Technology, 2010.
14. J. T. Gier and R. V. Dunkle, *Transactions of the Conference on the Use of Solar Energy*, The Scientific Basis, Tucson, October 31-November 1, 1955.
15. H. Tabor and I. T. Steinberger, *J Sci Instrum*, 1956, **33**, 356-358.
16. H. Tabor, *Sci Am*, 1956, **195**, 97-&.
17. R. B. Pettit, R. R. Sowell and I. J. Hall, *Sol Energ Mater*, 1982, **7**, 153-170.
18. D. P. Grimmer and R. K. Collier, *Sol Energy*, 1981, **26**, 467-469.
19. C. P. Lampert, in *Second Annual Conference on Absorber Surfaces for Solar Receivers*, Gounder, CO, 1979.
20. G. E. Mcdonald, *Sol Energy*, 1975, **17**, 119-122.
21. T. S. Sathiaraj, R. Thangaraj, H. Alsharbaty and O. P. Agnihotri, *Thin Solid Films*, 1991, **195**, 33-42.
22. T. S. Sathiaraj, R. Thangaraj, H. Alsharbaty, M. Bhatnagar and O. P. Agnihotri, *Thin Solid Films*, 1990, **190**, 241-254.

23. H. G. Craighead and R. A. Buhrman, *Appl Phys Lett*, 1977, **31**, 423-425.
24. H. C. Barshilia, N. Selvakumar, K. S. Rajam and A. Biswas, *J Appl Phys*, 2008, **103**.
25. B. Orel, Z. C. Orel and I. Radoczy, *Sol Energ Mater*, 1988, **18**, 97-107.
26. B. Orel, H. Spreizer, A. S. Vuk, M. Fir, D. Merlini, M. Vodlan and M. Kohl, *Sol Energ Mat Sol C*, 2007, **91**, 108-119.
27. B. Orel, H. Spreizer, L. Slemenik Perše, M. Fir, A. Šurca Vuk, D. Merlini, M. Vodlan and M. Köhl, *Sol Energ Mat Sol C*, 2007, **91**, 93-107.
28. C. A. Arancibia-Bulnes, C. A. Estrada and J. C. Ruiz-Suarez, *J Phys D Appl Phys*, 2000, **33**, 2489-2496.
29. N. Selvakumar and H. C. Barshilia, *Sol Energ Mat Sol C*, 2012, **98**, 1-23.
30. R. L. Champion and S. N. Laboratories, *Proceedings of the Line-focus Solar Thermal Energy Technology Development: A Seminar for Industry, Albuquerque, New Mexico, September 9, 10, 11, 1980*, National Technical Information Service, 1981.
31. R. B. Pettit and R. R. Sowell, *J Vac Sci Technol*, 1976, **13**, 596-602.
32. J. Salmi, J. P. Bonino and R. S. Bes, *J Mater Sci*, 2000, **35**, 1347-1351.
33. A. Andersson, O. Hunderi and C. G. Granqvist, *J Appl Phys*, 1980, **51**, 754-764.
34. Q. C. Zhang and D. R. Mills, *Appl Phys Lett*, 1992, **60**, 545-547.
35. G. A. Niklasson and C. G. Granqvist, *Sol Energ Mater*, 1983, **7**, 501-510.
36. H. G. Craighead, R. E. Howard, J. E. Sweeney and R. A. Buhrman, *Appl Phys Lett*, 1981, **39**, 29-31.
37. D. S. Gogova, *Mater Lett*, 1997, **30**, 109-113.
38. B. O. Seraphin, *Thin Solid Films*, 1976, **39**, 87-94.
39. V. Teixeira, E. Sousa, M. F. Costa, C. Nunes, L. Rosa, M. J. Carvalho, M. Collares-Pereira, E. Roman and J. Gago, *Thin Solid Films*, 2001, **392**, 320-326.
40. J. C. C. Fan and S. A. Spura, *Appl Phys Lett*, 1977, **30**, 511.
41. Q. C. Zhang and Y. G. Shen, *Sol Energ Mat Sol C*, 2004, **81**, 25-37.
42. Q.-C. Zhang, *Sol Energ Mat Sol C*, 2000, **62**, 63-74.
43. Z. Li, J. Zhao and L. Ren, *Sol Energ Mat Sol C*, 2012, **105**, 90-95.
44. X. X. Wang, H. F. Li, X. B. Yu, X. L. Shi and J. F. Liu, *Appl Phys Lett*, 2012, **101**.
45. I. T. Ritchie, S. K. Sharma, J. Valignat and J. Spitz, *Sol Energ Mater*, 1979, **2**, 167-176.
46. C. Nunes, V. Teixeira, M. L. Prates, N. P. Barradas and A. D. Sequeira, *Thin Solid Films*, 2003, **442**, 173-178.
47. Y. Yin, Y. Pan, L. X. Hang, D. R. McKenzie and M. M. M. Bilek, *Thin Solid Films*, 2009, **517**, 1601-1606.

48. W. Graf, F. Brucker, M. Köhl, T. Tröscher, V. Wittwer and L. Herlitze, *J Non-Cryst Solids*, 1997, **218**, 380-387.
49. S. N. Kumar, L. K. Malhotra and K. L. Chopra, *Sol Energ Mater*, 1983, **7**, 439-452.
50. T. Moller and D. Honicke, *Sol Energ Mat Sol C*, 1998, **54**, 397-403.
51. T. Boström, E. Wäckelgård and G. Westin, *Sol Energy*, 2003, **74**, 497-503.
52. T. Boström, E. Wäckelgård and G. Westin, *Sol Energ Mat Sol C*, 2004, **84**, 183-191.
53. T. Boström, S. Valizadeh, J. Lu, J. Jensen, G. Westin and E. Wäckelgård, *J Non-Cryst Solids*, 2011, **357**, 1370-1375.
54. B. Chen, D. F. Yang, P. A. Charpentier and S. Nikumb, *Sol Energ Mat Sol C*, 2008, **92**, 1025-1029.
55. H. C. Barshilia, P. Kumar, K. S. Rajam and A. Biswas, in *Sol Energ Mat Sol C*, 2011, **95**. 1707-1715.
56. D. Xinkang, W. Cong, W. Tianmin, Z. Long, C. Buliang and R. Ning, *Thin Solid Films*, 2008, **516**, 3971-3977.
57. J. Cheng, C. Wang, W. Wang, X. Du, Y. Liu, Y. Xue, T. Wang and B. Chen, *Sol Energ Mat Sol C*, 2013, **109**, 204-208.
58. A. Antonaia, A. Castaldo, M. L. Addonizio and S. Esposito, *Sol Energ Mat Sol C*, 2010, **94**, 1604-1611.
59. Z. Y. Nuru, C. J. Arendse, R. Nemutudi, O. Nemraoui and M. Maaza, *Physica B*, 2012, **407**, 1634-1637.
60. Q.-C. Zhang, *Journal of Vacuum Science & Technology A: Vacuum, Surfaces, and Films*, 1997, **15**, 2842-2846.
61. Q.-C. Zhang, *Sol Energ Mat Sol C*, 1998, **52**, 95-106.
62. Q.-C. Zhang, in *Proceedings of ISES World Congress 2007 (Vol. I – Vol. V)*, eds. D. Y. Goswami and Y. Zhao, Springer Berlin Heidelberg, 2009, pp. 1847-1853.
63. Q. C. Zhang, *J Phys D Appl Phys*, 1998, **31**, 355-362.
64. Q. C. Zhang, *J Phys D Appl Phys*, 2001, **34**, 3113-3120.
65. Q. C. Zhang, *Proceedings of Ises Solar World Congress 2007: Solar Energy and Human Settlement, Vols I-V*, 2007, 1847-1853.
66. Q.-C. Zhang, K. Zhao, B.-C. Zhang, L.-F. Wang, Z.-L. Shen, D.-Q. Lu, D.-L. Xie, Z.-J. Zhou and B.-F. Li, AVS, 1998, pp. 628-632.
67. D. A. G. Bruggeman, *Ann. Phys.*, 1935, **24**, 636-647.
68. S. X. Zhao and E. Wäckelgård, *Sol Energ Mat Sol C*, 2006, **90**, 1861-1874.
69. M. Nishimura and T. Ishiguro, *Jpn J Appl Phys*, 2004, **43**, 757-761.
70. J. A. Wang, B. C. Wei, Q. R. Wei and D. J. Li, *Phys Status Solidi A*, 2011, **208**, 664-667.
71. S. Esposito, A. Antonaia, M. L. Addonizio and S. Aprea, *Thin Solid Films*, 2009, **517**, 6000-6006.

72. F. Garnich and E. Sailer, *Sol Energ Mater*, 1990, **20**, 81-89.
73. M. Okuyama, K. Furusawa and Y. Hamakawa, *Sol Energy*, 1979, **22**, 479-482.
74. W. Brünger, *Vacuum*, 1980, **30**, 125-127.
75. M. Farooq, A. A. Green and M. G. Hutchins, *Sol Energ Mat Sol C*, 1998, **54**, 67-73.
76. P. K. Gogna and K. L. Chopra, *Sol Energy*, 1980, **23**, 405-408.
77. O. P. Agnihotri, B. K. Gupta, A. K. Agarwal and V. P. Bhatnagar, *Thin Solid Films*, 1983, **109**, 193-200.
78. Q.-C. Zhang, M. S. Hadavi, K.-D. Lee and Y. G. Shen, *Journal of Physics D: Applied Physics*, 2003, **36**, 723.
79. R. C. Juang, Y. C. Yeh, B. H. Chang, W. C. Chen and T. W. Chung, *Thin Solid Films*, 2010, **518**, 5501-5504.
80. N. Selvakumar, N. T. Manikandanath, A. Biswas and H. C. Barshilia, *Sol Energ Mat Sol C*, 2012, **102**, 86-92.